

Origin of Metal-Insulator Transitions in Correlated Perovskite Metals

M. Chandler Bennett,^{1,*} Guoxiang Hu,^{2,†} Guangming Wang,³ Olle Heinonen,⁴ Paul R. C. Kent,⁵ Jaron T. Krogel,^{1,‡} and P. Ganesh^{6,§}

¹*Materials Science and Technology Division, Oak Ridge National Laboratory, Oak Ridge, Tennessee 37831, USA*

²*Department of Chemistry and Biochemistry, Queens College, City University of New York, Flushing, NY 11367, USA*

³*Department of Physics, North Carolina State University, Raleigh, North Carolina 27695, USA*

⁴*Materials Science Division, Argonne National Laboratory, Chicago, Illinois USA*

⁵*Computational Sciences and Engineering Division, Oak Ridge National Laboratory, Oak Ridge, Tennessee 37831, USA*

⁶*Center for Nanophase Materials Sciences, Oak Ridge National Laboratory, Oak Ridge, Tennessee 37831, USA[§]*

(Dated: January 26, 2022)

The mechanisms that drive metal-to-insulator transitions (MIT) in correlated solids are not fully understood, though intricate couplings of charge, spin, orbital, and lattice degrees of freedom have been implicated. For example, the perovskite SrCoO₃ is a FM metal while the oxygen-deficient (*n*-doped) brownmillerite SrCoO_{2.5} is an anti-ferromagnetic (AFM) insulator. Given the magnetic and structural transitions that accompany the MIT, the driving force for such a MIT transition is unclear. We also observe that, interestingly, the perovskite metals LaNiO₃, SrFeO₃, and SrCoO₃ also undergo MIT when *n*-doped via high-to-low valence compositional changes i.e. Ni³⁺ → Fe⁴⁺, Sr²⁺ → La³⁺, and Sr²⁺ → La³⁺, respectively. On the other hand, pressurizing the insulating brownmillerite SrCoO_{2.5} phase, drives a gap closing. Here we demonstrate that the ABO₃ perovskites most prone to MIT are self-hole doped materials, reminiscent of a negative charge-transfer metal, using a combination of density functional and fixed-node diffusion quantum Monte Carlo calculations. Upon *n*-doping the negative-charge transfer metallic phase, an underlying charge-lattice (or electron-phonon) coupling drives the metal to a charge and bond-disproportionated gapped insulating state, thereby achieving ligand hole passivation at certain sites only. The size of the band gap is linearly correlated with the degree of hole-passivation at these ligand sites. Further, metalization via pressure is also stabilized by a similar increase in the ligand-hole, which in turn stabilizes the ferromagnetic coupling. These results suggest that the interaction that drives the band gap opening to realize a MIT even in correlated metals is the charge-transfer energy, while it couples with the underlying phonons to enable the transition to the insulating phase. Other orderings (magnetic, charge, orbital etc.) driven by weaker interactions may assist gap openings at low doping levels, but it is the charge-transfer energy that predominantly determines the band gap, with a negative energy preferring the metallic phase. This *n*-doping can be achieved by modulations in oxygen-stoichiometry or metal-composition or pressure. Hence, controlling the amount of the ligand-hole, set by the charge-transfer energy, is the key-factor in controlling MIT.

I. INTRODUCTION

The metal-insulator transition (MIT) in various strongly correlated transition-metal oxides is essential for recently proposed device applications, for instance memristors for next-generation neuromorphic computing[1–4]. However, understanding the underlying mechanism of the MIT in correlated solids has been a longstanding problem [5, 6], making selection and optimization of appropriate materials difficult. The theoretical difficulty in analyzing these materials lies in the strong electron correlation, giving rise to complex many-body phenomena and a close coupling of charge, spin, orbital, and lattice degrees of freedom. Identification of the important variables and key interactions that influence the MIT in

correlated metals has consequently remained elusive.

The ABO_x perovskite family has several candidate compounds that undergo a sharp and tunable MIT[7–11], which forms an excellent playground to look for the driving forces behind the transition. For example, consider the oxygen-rich perovskite SrCoO₃ (PV-SCO) which is a correlated ferromagnetic (FM) metal. The introduction of oxygen-vacancies typically amounts to introducing negative charge-carriers (i.e. *n*-doping). In a conventional band-theory picture, such doping often increases electronic conductivity, but in PV-SCO it leads to an insulating ground-state with a concomitant change in the magnetic ordering[12, 13]. Indeed, the oxygen-deficient brownmillerite SrCoO_{2.5} (BM-SCO) is an anti-ferromagnetic insulator. However, under pressure (both uniform and uniaxial), this anti-ferromagnetic insulator shows a reduction in the electronic band gap by 40%[14]. Recent experiments[15] suggest that under pressure, the number of holes on oxygen-ligands possibly increase, which in principle could stabilize a ferromagnetic coupling between the metal-ions, in turn eventually closing

* bennettcc@ornl.gov

† ghu@qc.cuny.edu

‡ krogeljt@ornl.gov

§ ganeshp@ornl.gov

the band-gap in BM-SCO. Given the concomitance of the MIT to structural or magnetic transitions (or both), it is not immediately clear what would be the key change that triggers the MIT in PV-SCO and other similar correlated perovskite metals. Furthermore, it is not clear whether the gap opening is driven by Hubbard repulsive interactions from correlated electrons in the $3d$ orbitals, hybridization of orbitals between covalently bonded atoms, magnetic exchange interactions that favor Hund's rule, or charge-transfer energies that determine the transfer of electrons from the ligand (anion) to the metal (cation) sites.

The family of rare-earth nickelates is another example where the MIT occurs concomitantly with structural and magnetic transitions [16–18]. While the size of the rare-earth tunes the transition temperature, the underlying mechanism appears to remain the same and is dependent on the metal-ligand bonding[19]. In all the nickelate compounds, the high-temperature phase is a correlated metal with fluctuating magnetic moments (i.e. the paramagnetic phase). Below a certain temperature, all compounds, except for LaNiO_3 , transition into a bond-disproportionated phase, i.e. a phase with alternating long and short Ni-O bonds. Some compounds exhibit an additional transition to an anti-ferromagnetic (AFM) phase concomitant to this bond-disproportionation. For example, recent experiments suggest even LaNiO_3 undergoes such an AFM transition below $\sim 157\text{K}$ [20]. Similarly, n -doping with hydrogen induces a metal-to-insulator transition in SmNiO_3 , with the underlying mechanism still uncertain with the observation of local lattice distortions in the insulating phase [21, 22]. Based on the Zaanen-Sawatzky-Allen (ZSA) classification scheme[23], the nickelates are self-hole doped Mott insulators where the self-hole doping is due to a negative charge-transfer energy.

Due to a forced high-valence cationic-state (Ni^{3+} , d^7), the high-temperature metal is stabilized by self-hole doping (d^8L , where L indicates a ligand-hole) and upon reducing the temperature, a *bond* disproportionated insulating state emerges instead of a *charge* ordered state, with short and long Ni-O bonds stabilizing alternating d^8L^2 and d^8L^0 Ni-cations, that in some cases also stabilizes an anti-ferromagnetic ground-state. As such, while a Hubbard repulsion is necessary, it is not sufficient to transition to an insulating phase. Indeed, even in conventionally well regarded Mott insulators, such as VO_2 and NiO , and their superlattices, we recently demonstrated that that charge-state of oxygen anions and its coupling to local structural distortions play a significant role in driving the MIT [24–29]. Though, it is still not very clear why self hole-doping leads to a bond disproportionated phase when temperature is reduced which opens a gap, and how the ZSA theory generalizes to MIT driven by changes in pressure, composition, and stoichiometry.

To address this question, we posit that the connection of the MIT and bond-disproportionation extends beyond the nickelate family of perovskites and is not limited to

MITs triggered by a change in temperature. Similar to the nickelates, the ferrates and the cobaltates have metal-ions forced in high-valency as well, e.g. Fe^{4+} in SrFeO_3 and Co^{4+} in SrCoO_3 , and thereby possess large electron affinities leading to a low, possibly negative, charge-transfer[30, 31] energy. Hence, these systems should also exhibit self-hole doping to stabilize their metallic phase. We note that the MIT can also be triggered by compositional changes. Just as n -doping PV-SCO by making it non-stoichiometric opens a band gap in the Brownmillerite phase, similarly n -doping PV-SCO by substituting Sr^{2+} for La^{3+} also leads to a band gap opening. Similarly, LaFeO_3 is an insulator and can be regarded as an n -doped PV- SrFeO_3 ($\text{Sr}^{2+} \rightarrow \text{La}^{3+}$). Given these observations, we hypothesize that metallic ABO_3 perovskites that demonstrate a MIT are self-hole doped negative charge transfer metals in the Zaanen-Sawatzky-Allen (ZSA) classification scheme. n -doping such self-hole doped metals fills these pre-existing holes and gives rise to an insulating state, possibly via a charge-lattice (or equivalently an electron-phonon) coupling, leading to a bond-disproportionated insulating structure, that owing to a symmetry lowering transition necessarily is also charge-disproportionated (not necessarily charge-ordered). Magnetic ordering as well as other kinds of ordering, such as charge- or orbital-ordering may further assist in the gap opening of this bond-disproportionated phase.

To prove the conjecture made above, in this work, we use density functional theory based methods together with the highly accurate fixed-node diffusion Monte Carlo (FN-DMC)[32] flavor of quantum Monte Carlo (QMC)[33] to quantitatively compare the degree of self-hole doping in perovskite metals, and how it correlates with changes in metal-composition, oxygen-stoichiometry and pressure, across a MIT. As a measure of the degree of self-hole doping, i.e. $d^{n+1}L$, we compare calculations of oxygen occupations via integrated densities around the oxygen sites. We additionally demonstrate that changes in the degree of self-hole doping triggers a charge-lattice instability. To benchmark our approach, we perform FN-DMC calculations of various ground-state properties and compare to experiments where possible, finding very good agreement. The ground-state properties used for comparison are the cohesive energies of the perovskite compounds – indicates accuracy of describing atomic bonding – and the local magnetization around the metal-site which is important in determining the spin-state of the metallic cation. A high quality description of the ground state is foundational for our investigations of charge-transfer in the perovskite family of materials considered here. The fundamental band gaps from FN-DMC-benchmarked DFT+ U calculations are also in good agreement with available experimental gaps, with FN-DMC-gaps showing similar trends across the different compounds. We find that holes are present in the oxygen-site for correlated perovskite metals (as measured by the reduced oxygen occupations rel-

ative to the insulating compounds), and that transitioning to a gapped insulating phase via changes in metal-composition or oxygen-stoichiometry or pressure results in a reduction of the holes on oxygen-sites (increased oxygen occupation). This is consistent with our density of states calculations, where the metals have an unoccupied p band, while insulators resulting from these metals undergoing an MIT have a p - d type band gaps. We find strong evidence for the insulating phases to be bond-disproportionated, due to an underlying charge-lattice coupling. We therefore prove our conjecture that self-hole doped correlated metals can trigger a metal-to-insulator transition by n -doping into their unsaturated holes (increased oxygen occupation) due to a strong charge-lattice (or electron-phonon) coupling in perovskites, and that this n -doping can be achieved by changes in oxygen-stoichiometry, metal-composition, or pressure. Hence, controlling the ligand-hole population, set by the charge-transfer energy, is the key-factor in controlling MIT, even in correlated perovskite metals with strong on-site Hubbard interactions.

II. METHODS

We perform a combined study using density functional theory (DFT) with a linear-response determined Hubbard U (i.e. U_{LR})[34] as well as fixed-node diffusion Monte Carlo (FN-DMC) calculations to obtain ground-state properties (details available in the supplementary information). Computations were performed for metallic SrCoO₃ and LaNiO₃ compounds as well as the insulating LaFeO₃ and LaCrO₃ compounds in the perovskite phase and SrCoO_{2.5} in the brownmillerite phase, at pressures ranging from 0-8 GPa. The magnetic orderings of the experimental ground state were considered, namely ferromagnetic for SrCoO₃ and LaNiO₃; antiferromagnetic (AFM) for LaFeO₃, LaCrO₃, LaNiO₃ and BM SrCoO_{2.5}. For the insulating phases, we also calculated the optical gap using LDA+ U_{LR} and FN-DMC. The nodal surfaces for FN-DMC were obtained by using the variational property of FN-DMC and varying the strength of the metal-site Hubbard interaction within the LDA+ U to find the best nodal surface for each material. For the BM-SCO phase, distinct U values were assumed for the two different coordination sites of the Co-atom. For PV-SCO, we additionally used nodal surfaces obtained by varying the exact exchange fraction w with PBE0 _{w} .

For this work, we utilized the QUANTUM ESPRESSO suite[35] and the VASP package[36–39] for the DFT+ U calculations and for generating the orbitals needed for QMC. All QMC calculations were performed with the high-performance QMCPACK code[40, 41]. Using the NEXUS suite[42], reproducible workflows were written for the DFT calculations and the complete set of calculations needed for QMC. Input and output files for the calculations performed in this study are available and maintained at the Materials Data Facility[43].

III. RESULTS & DISCUSSION

A. Implications of ground state energies and magnetic structure

Tables I and II compare the cohesive energies and the local-moments computed from FN-DMC to available experiments, respectively. Cohesive energy has contributions from all necessary interactions, and is often incorrect in standard DFT-calculations [44]. Here we find that the cohesive energies for LaNiO₃, LaFeO₃, and LaCrO₃ are in good agreement with estimates from the literature (derivations of experimental cohesive energies is provided in the supplemental material). Particularly, we find that the inclusion of spin-polarization is necessary to bring the cohesion of LaNiO₃ in closer agreement with experimental estimates, suggesting that the physics that stabilizes the local moment is essential in describing its electronically metallic state. The accuracy in cohesive energies for both metals and insulators indicates that FN-DMC is appropriate for looking at the driving force behind the MIT. In addition to cohesive energies, the methodology also captures the magnitude of the local moments and its change with coordination and structure type for the cobaltates, with absolute values very close to the values obtained from spin-polarized neutron scattering experiments in the literature[20, 45, 46]. This affirms our methodology to predict the underlying electronic structure, allowing us to meaningfully conclude from systematic changes observed in charge-/spin-densities, and derived quantities computed from the FN-DMC estimated many-body ground-state wave function.

TABLE I: Cohesive Energies from DMC in units of eV/atom.

Material	DMC	Exp.
SrCoO ₃	4.412(6)	
LaNiO ₃ (NM)	5.512(6)	5.760 ^a
LaNiO ₃ (FM)	5.656(8)	
LaFeO ₃	6.220(6)	6.120 ^a
LaCrO ₃	6.400(6)	6.422 ^a

^a See supplemental material for derivations of experimental values.

Rhombohedral LaNiO₃ was thought to be a paramagnet, until very recent experiments on single-crystals of LaNiO₃ demonstrates that it undergoes a transition to an anti-ferromagnetic phase below ~ 157 K, while still remaining metallic[20]. Nevertheless, the measured local moment was $\sim 0.3\mu_B$, much smaller than the moments on other perovskite systems, in good qualitative agreement with trends observed from our FN-DMC calculations, which even in the ferromagnetic phase of rhombohedral LaNiO₃ finds a lower moment of $\sim 1.02\mu_B$ (Table II) compared to other perovskite magnets. Note that our FN-DMC moment for the G-type AFM ordering of LaNiO₃ was also small ($\sim 0.52\mu_B$), however, this ordering

TABLE II: Local Magnetic moments (Bohr mag) of cations from FN-DMC. The local moments are calculated by spherically averaging the $\rho_{\text{up}} - \rho_{\text{down}}$ density (where $\rho_{\text{up/down}}$ is the spin-up/spin-down density) around the cation site.

Material	Atom	DMC	Exp.
SrCoO ₃	Co	2.563(1)	2.5
LaNiO ₃ (FM)	Ni	1.019(1)	0.3 ^a
LaNiO ₃ (G-AFM)	Ni	0.518(2)	
SrCoO _{2.5}	Co1	3.187(1)	3.12(13) ^b
SrCoO _{2.5}	Co2	3.081(1)	2.88(14) ^b
LaFeO ₃	Fe	4.202(1)	4.6(2) ^c
LaCrO ₃	Cr	2.537(2)	2.8(2) ^c

^a Reference [20]

^b Reference [46]

^c Reference [45]

was not energetically favored in FN-DMC over FM ordering. In all cases, we have used spin symmetry-broken trial wavefunctions in FN-DMC, which may partially explain the larger fluctuations observed when the predicted moments are small in magnitude. The local moments of all other compounds from our fully *ab initio* DMC calculations, including those on the different Wyckoff positions for the Brownmillerite phase, show excellent agreement with experiments.

The on-site moments may be understood qualitatively in the atomic limit as $\sim 2\sqrt{s(s+1)}$, where s is the spin multiplicity, we find that the metal-sites under an octahedral crystal-field splitting are close to a high-spin configuration for LaCrO₃ ($t_{2g}^3 e_g^0$) and LaFeO₃ ($t_{2g}^3 e_g^2$), an intermediate spin state for SrCoO₃ ($t_{2g}^4 e_g^1$) and a low-spin state for LaNiO₃ ($t_{2g}^6 e_g^1$). Interestingly, both linear-response theory as well as FN-DMC orbital optimization predicts an increasing trend in the strength of the on-site Hubbard repulsion for 3d electrons as we increase the d -orbital filling from LaCrO₃ to LaFeO₃, but it is reduced slightly as we move to SCO and LNO (details in SI). But the variation overall is not large and both the U_{LR} and the U_{DMC} remain between 4-5.5 eV. Further, the band gaps do not follow the trend of the Hubbard interaction, with LaCrO₃ having a larger gap than LFO, and the SCO with similar value for the Hubbard interaction as LaCrO₃ showing a metallic phase. This suggests that while the Hubbard interaction parameter (including the magnetic exchange, which dictates the Hund's rule) is necessary to stabilize the spin-state, and determine the local moment, the opening of the band gap is determined in large measure by other interactions, such as charge-transfer. Further, the responsible interaction necessarily also destabilizes the high-spin state favored by Hund's rule in both SCO and LNO. Because all compounds have the same oxygen ligand, one way to assess the degree and nature of charge-transfer across these compounds is to compare the charge associated with it.

B. Understanding key ligand charge behavior

To understand what type of charge-transfer could be present in our systems, we next compare the charges on the oxygen ligand sites. The charges were computed by integrating the radial charge-density around oxygen atoms within a fixed radius for all compounds, from both the linear-response LDA+ U_{LR} as well as the FN-DMC following a nodal optimization using LDA+ U orbitals. The computed charges are in good agreement between the different methods (see SI Tables III-V), suggesting that the linear-response captures the bonding characters in the solid appreciably well. As also seen in Figure 1, the LDA+ U_{LR} band gaps are in decent agreement with the experimental gaps. A high degree of charge-transfer from oxygen-ligands to the metal-site is indicative of a negative charge-transfer energy. This is what we observe from Fig.1a and 1b, where the metallic SCO and LNO are seen to have lowest relative charges on the oxygen atoms compared to the mean or majority charges carried by the oxygen ligand amongst all the compounds. Interestingly, the change in the majority charge on the oxygen ligand correlates linearly with the band gap, irrespective of whether we consider the observed experimental gap, or the band gaps calculated via LDA+ U_{LR} or LDA+ U_{DMC} , and in spite of the change in the structure from perovskite to a brownmillerite phase. This clearly suggests that the quantity determining the size of the band gap across MIT in correlated perovskites is the charge-transfer energy, and that the metals are self-hole doped because it is negative.

A negative charge-transfer energy will also lead to a change in the formal oxidation state of the metal site, and thereby the magnetic moment. For example, in PV-SCO, the nominal Co⁴⁺ ($3d^5$) valency will get lowered due to a transfer of electron from the ligand to the metal-site, destabilizing the nominally high-spin $t_{2g}^3 e_g^2$ state, and giving rise to an intermediate spin-state $t_{2g}^4 e_g^1$ with a net moment less than $\sim 3\mu_B$, which would be in good agreement with both experiments and our calculations (Table II). Our integrated charges around the Co-site also supports this conclusion, with the nominal valency of ~ 2.65 a.u., closer to a Co³⁺ as shown in Table SI-???. Similarly, hole-doping is seen to lower the nominal Ni³⁺ to be ~ 1.73 a.u., closer to Ni²⁺. With a reduced valency, it would be possible to stabilize a low-spin state, such as $t_{2g}^6 e_g^2$, explaining the low moments in both the measured and our computed values. Note that this would also require the holes to have an e_g symmetry so as to quench the high-spin moments in the e_g sub-bands of the Co and Ni-atoms. As we will see below, this is just what we observe.

While the nominal charges are much reduced for the metallic PV-SCO and PV-LNO, consistent with a negative charge-transfer picture, the insulating perovskites have a charge-state closer to the nominal valency e.g a valency of 3+ in LaFeO₃ (2.50 a.u.) and LaCrO₃ (2.78 a.u.) (Table SI-??). Nominally, an isolated oxygen atom possesses 6 a.u. of charge. We note that our pseudopo-

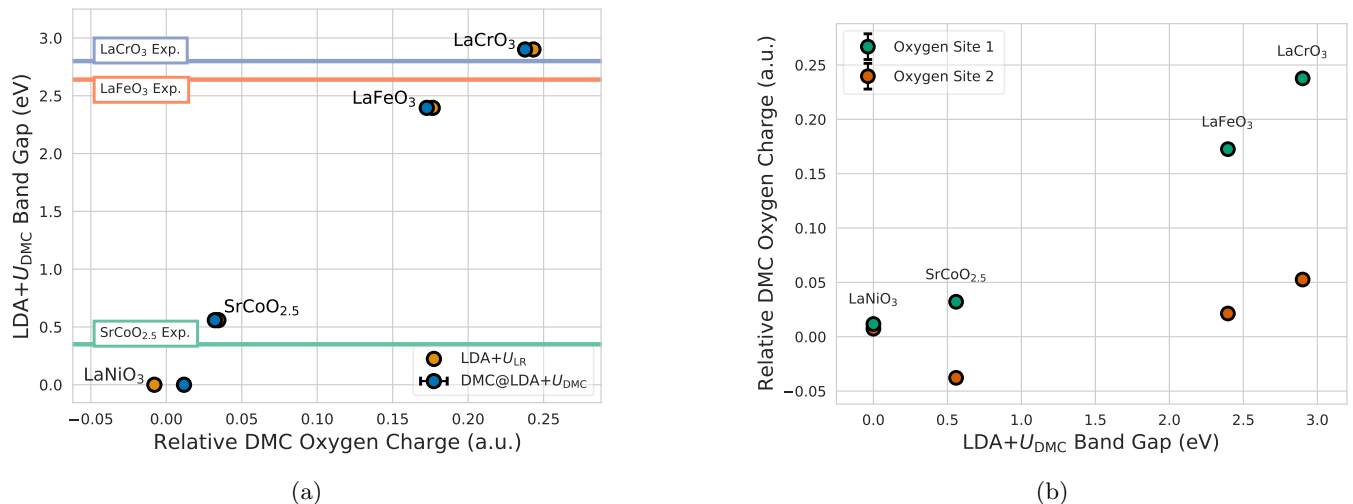


FIG. 1: (a) For LaNiO₃, SrCoO_{2.5}, LaFeO₃, and LaCrO₃, optical band gaps calculated within LDA+ U versus the DMC cumulative radially-averaged charge around the oxygen site relative to SrCoO₃ (with O-charge 6.4120 a.u.). The oxygen site with majority charge was used for each system and the value of U that minimizes the FN-DMC energy is chosen for each system. Cumulative charges are also shown from LDA+ U with U values consistent with DMC. For comparison, we indicate experimentally measured band gaps for the insulating systems (SrCoO_{2.5}[47], LaFeO₃[48], and LaCrO₃[49]) with horizontal solid lines. (b) LDA+ U_{DMC} band gap versus site-specific cumulative radially-averaged charge around the oxygen site relative to SrCoO₃.

tentials use a 2-electron core for oxygen and a 10-electron core for the 3d metals. Due to formation of metal-ligand bonding, and owing to its high electronegativity, oxygen atoms are seen to possess more than 6 a.u. of charge for the compounds. Remarkably, the amount of oxygen-ligand charge appears to be the same (6.41 a.u.) for the two metallic systems – PV-SCO and PV-LNO, even though the total charges on the metal-sites (Co & Ni) are very different (14.35 & 16.27 a.u.) (see Table SI-??). This again underscores the importance of the anion $O-p$ states in determining the overall electronic-structure. Magnetic transitions could in certain cases result from a MIT, such as in PV-SCO – but do not primarily drive it. Indeed, even LaNiO₃ was found to be a metal, a rarity for a material with an AFM ground state, consistent with experiments. This difference relative to broadly observed FM correlated metals suggests that modified magnetic interactions that could result in a particular type of AFM ordering for LaNiO₃ and FM for other materials may not be the primary determinant for gap opening in self hole-doped **perovskite** metals. Given that the gap varies monotonically with the formal electronegativity of the metal-atom (see Fig. SI-??), it is clear that the opening of the gap in these self hole-doped metals would require changing the nature of this charge-transfer energy, i.e making it more positive as the gap increases.

To investigate how the nature of the gap changes, we look at the orbitals participating in the gap opening. If there is an energy cost to transfer charges from the $O-p$ orbitals to the metal- d orbitals, then the system would be gapped. Such a gap is naturally realized when the

Fermi-level moves from the middle of the $O-p$ band, such as the case in the self-hole doped metals, to the top of the $O-p$ -band, giving rise to a $p-d$ type gap. A larger Hubbard interaction would naturally yield a larger $p-d$ gap. Indeed, as shown in the calculated projected density-of-states, Fig. SI-?? in SI, both metallic SCO and LNO show a relatively large number of states with an $O-p$ character at the Fermi-level. As we move out of this metallic phase by reducing the amount of charge-transfer from $O-p$ to the metallic d state, by stoichiometrically or compositionally n -doping it, a gap is opened in the insulators BM-SCO (Fig. 3) and LaFeO₃ (Fig. SI-??). These compounds show a $p-d$ type band gap, reminiscent of a more positive charge-transfer system. As we further move to LaCrO₃, the amount of charge on the ligand site further increases, with the Cr-metal showing a more formal oxidation state of +3, as noted above. At this point the band-gap is equally determined by the Hubbard interaction and the charge-transfer energy, as also evidenced in the increased d contribution to the valence-state in the projected density-of-states (Fig. SI-??).

The charge-difference with respect to a self-hole doped metal indicates how the density would respond to electron doping such a metal, and represents the nature of the lowest excitation. This is clearly seen when we plot the DMC charge-density isosurfaces, localized around the oxygen sites as shown in Fig. 2a for the different compounds, in reference to the metallic PV-SCO. While the difference between metallic LNO and SCO shows the hole to have more of a t_{2g} -symmetry, the gapped insulators show the hole state to have more of an e_g symmetry. This

is exactly what we expect, because for the self-hole doping to destabilize the high-spin states in the metallic SCO and LNO, as discussed above, the states involved in the electron-transfer need to have an e_g symmetry. Further, with increasing n -doping the magnitude of this charge-transfer increases, suggesting that the charge-transfer energy is becoming more positive. Thinking of this charge-density difference as the lowest type of excitation from the sea of electrons in the self hole-doped metal to form an n -doped insulator, we see that the nature of this excitation is $p-d$ -like, in agreement with the predominantly $p-d$ like gaps we observe for all systems in their density-of-states (Fig. SI-??). These observations suggest that n -doping a negative charge-transfer metal can result in making the charge-transfer energy more positive. However, it is not clear if n -doping simply shifts the Fermi-level to open a band gap when the Fermi-level reaches the top of the p -band or if there is some kind of instability that opens a gap when the system is perturbed away from its self-doped metallic state.

Notice that while the majority charge on the oxygen ligand showed a monotonic increase with n -doping the self hole-doped metal, the compounds show a symmetry lowering transition, which we can also associate with charge-disproportionation. Indeed, while one of the oxygen-ligand site shows an increase in charge (Fig. 1b), the others have the same electron count as in the metallic phase. Also, a shorter metal-ligand bond length is associated with an oxygen site with less charge in all the compounds we have investigated, as shown in Table SI-?. This suggests a clear connection between charge and bond disproportionation. Interestingly enough, as the band-gap increases, the amplitude of the charge disproportionation also increases. Without further information, it is not immediately clear if the charge disproportionation is caused by the bond disproportionation or vice versa, and what if any is its role in opening the band gap. But it is clear that under n -doping when a self-hole doped metal undergoes an insulating transition, symmetry is always lowered.

C. Charge-lattice coupling in SrCoO₃

To further understand this connection between charge and bond disproportionation, and explain the symmetry lowering, we subjected cubic SrCoO₃ to the same level of electron doping ($0.25 e^-/\text{Co}$) as the largest radial charge transfer we observed in our study. Interestingly, as shown in Fig. 2b, n -doped PV-SCO shows a phonon-instability. The instability is at an R point of the Brillouin zone, corresponding to an octahedral rotation. Indeed, a similar R type octahedral rotation underlies the ground-state structure of LaFeO₃, leading to its rhombohedral symmetry. Freezing the octahedral rotation lowers the energy, as seen in Fig. 2c, suggesting a weak, but persistent charge-lattice (i.e. electron-phonon) coupling. Similarly, hole-doping LaFeO₃ also gives rise to a phonon instabil-

ity (Fig. SI-??). This suggests that as the correlated metal becomes n -doped, either via removing oxygen-atoms or chemical substitution (or by applying strain as discussed below), the system undergoes bond disproportionation due to the underlying charge-lattice coupling, which in turn can lead to a charge disproportionated state as the symmetry gets lowered. Indeed, even in hole-doped correlated metals that show a charge-ordered ground state, phonon damping and changes in heat conduction have been experimentally observed, supporting this thesis [50]. Such bond and charge disproportionation can remove electronic degeneracies and stabilize other symmetry breaking transitions such as magnetic, charge-ordering or orbital-ordering, eventually opening a band gap.

While we demonstrated how a self-hole doped metal can become an insulator due to change in metal-composition and oxygen-stoichiometry, pressure can achieve the same result. Indeed, a recent experiment suggests that pressurizing the antiferromagnetic BM-SCO phase leads to a reduction in the band-gap [14]. While beyond 8.5 GPa the system appeared to transform into a different structure, up to 8.5 GPa a monotonic reduction in the optical gap was seen with pressure without any structural change. Indeed, BM-SCO is an insulator in the antiferromagnetic phase but a metal in the ferromagnetic phase, as seen in our density-of-states plot in Fig. 3c. By plotting the enthalpy difference between the two magnetic orderings as a function of strain induced by pressure (Fig. 3a), we find that the FM-ordering becomes more stable at higher pressures. Further investigating the amount of holes on the O- p orbitals, we find that with pressure the amount of charge on the oxygen ligand sites decrease monotonically. The charges were computed within the same radius, scaled to the reduction in volume, shown in Fig. SI-?. A decrease in the charges indicate an effective increase in the amount of O- p holes. Presence of such holes can stabilize the ferromagnetic coupling between the Co-sites, as shown in Fig. 3b. Indeed, small local moments observed on the O- p sites ($0.17 \mu_B$) had an opposite orientation to the ferromagnetically coupled moments on the Co-site. This clearly suggests, that the reduction in the band gap and its eventual closing under the application of pressure in BM-SCO insulator is also driven by the same charge-transfer energy, with compressive (tensile) strain acting as p (n)-doping of the system which thereby modifies the ligand holes, and that the AFM ordering in unstrained BM-SCO is a secondary effect that further assists in stabilizing the gap. Our findings also elucidate the physics underpinning recently observed machine-learning based identification of the average deviation of covalent radii and the global instability index as features that predominantly correlate with the tendency of materials to undergo a thermally driven MIT [51].

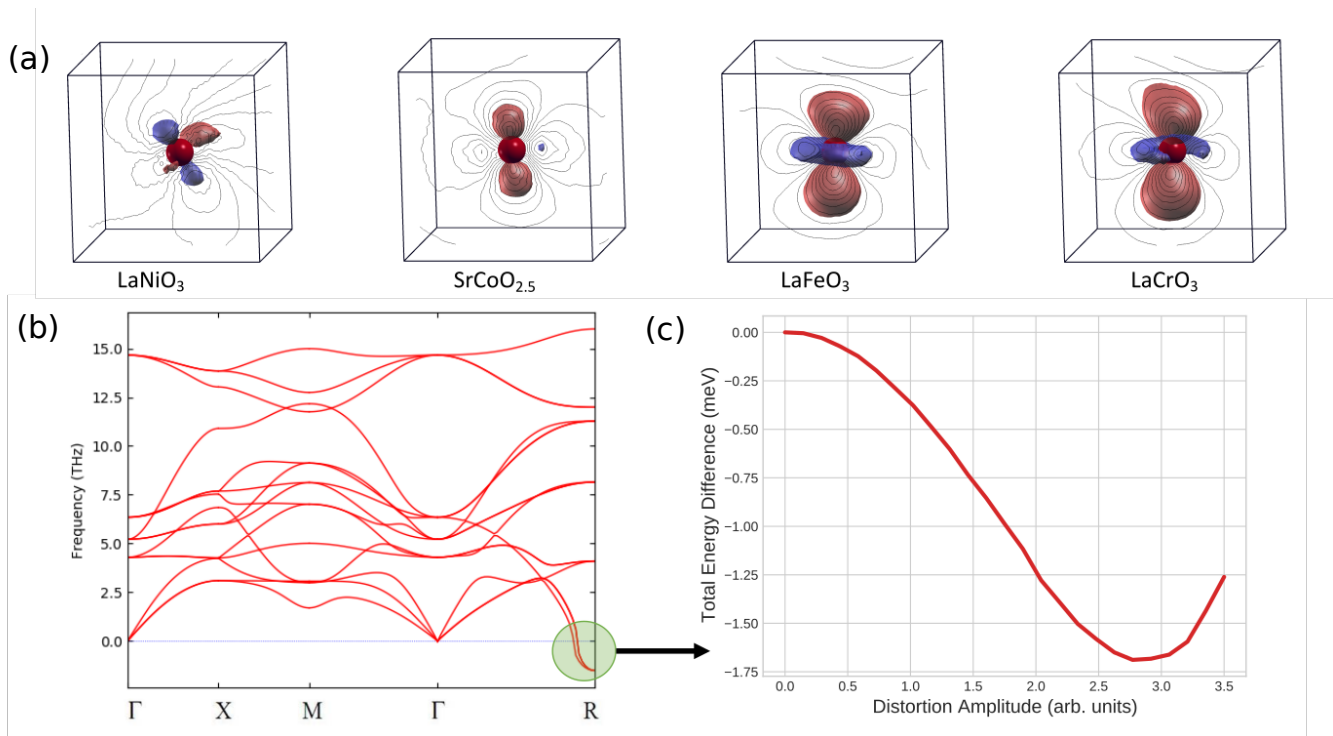


FIG. 2: (a) DMC charge-density isosurface differences for the indicated compounds with respect to PV-SCO plotted around an apical O-atom. An increase in charge is shown in ‘red’ while a decrease in ‘blue’. For each of the isosurfaces, the oxygen atom is centered in a cube of length 1.4 Å and we take an isovalue of 0.022 a.u. so that each graphic can be soundly compared. (b) Phonon bands for e^- -doped PV-SCO showing dynamic instability at the R -point corresponding to an octahedral rotation. (c) Energy-surface along the distortion corresponding to the instability at the R -point suggesting a tendency for bond-disproportionation due to charge-disproportionation.

IV. CONCLUSIONS

In this work, we use density functional theory based methods and the diffusion Monte Carlo (DMC) flavor of the many-body quantum Monte Carlo (QMC) approach that explicitly treats strong electron-electron correlations, to understand what drives MIT in correlated perovskites. Where experimental data is available, comparisons cohesive energies, local moments and other quantities are made. We find the correlated metal such as PV-SCO and PV-LNO to be self-hole doped as measured by significant O_p contributions to conduction bands and decreased oxygen occupation relative to the studied insulators, with similar amounts of ligand-hole. The electronic band gap in insulating compounds that are related to these self-hole doped metals via n -doping, due to changes in oxygen-stoichiometry such as SrCoO_{2.5}, or metal-compositions, such as, LaFeO₃ and LaCrO₃, show filling of this ligand-hole in some sites, with the gap nearly linearly changing with the degree of average (or majority) filling, suggesting that the band gap is opened by charge-transfer energies. Further, the insulating phases are shown to be *both* charge and bond-disproportionation due to an underlying charge-lattice coupling, with more ligand-holes on certain

oxygen-sites than others in the symmetry lowered bond-disproportionated phase. The charge-disproportionation drives bond-disproportionation, as is seen from phonon instabilities that arise when n -doping a pristine cubic perovskite phase. Together, this leads to the opening of a band gap, that is more p - d like beyond a critical amount of n -doping, transitioning of a self-hole doped metal to a less self-hole doped insulator. Similarly, we find that pressure leads to an increase in ligand holes in the oxygen-sites, driving a transition to a ferromagnetic metallic ground-state.

Our study thus suggests that self-hole doped correlated metals can trigger a metal-to-insulator transition by n -doping into a less self-hole doped insulator as doping makes the charge-transfer energy more positive, and that this can lead to symmetry lowering transitions due to a strong charge-lattice (or electron-phonon) coupling. This n -doping can be achieved by modulations in oxygen-stoichiometry or metal-composition or pressure. Moreover, this tendency to remain self-hole doped in correlated metals determines a universal electronic response to modulations in oxygen-stoichiometry/metal-composition/pressure via the charge-lattice coupling. Hence, controlling the amount and anisotropy of the ligand-hole is the key-factor in controlling MIT even in

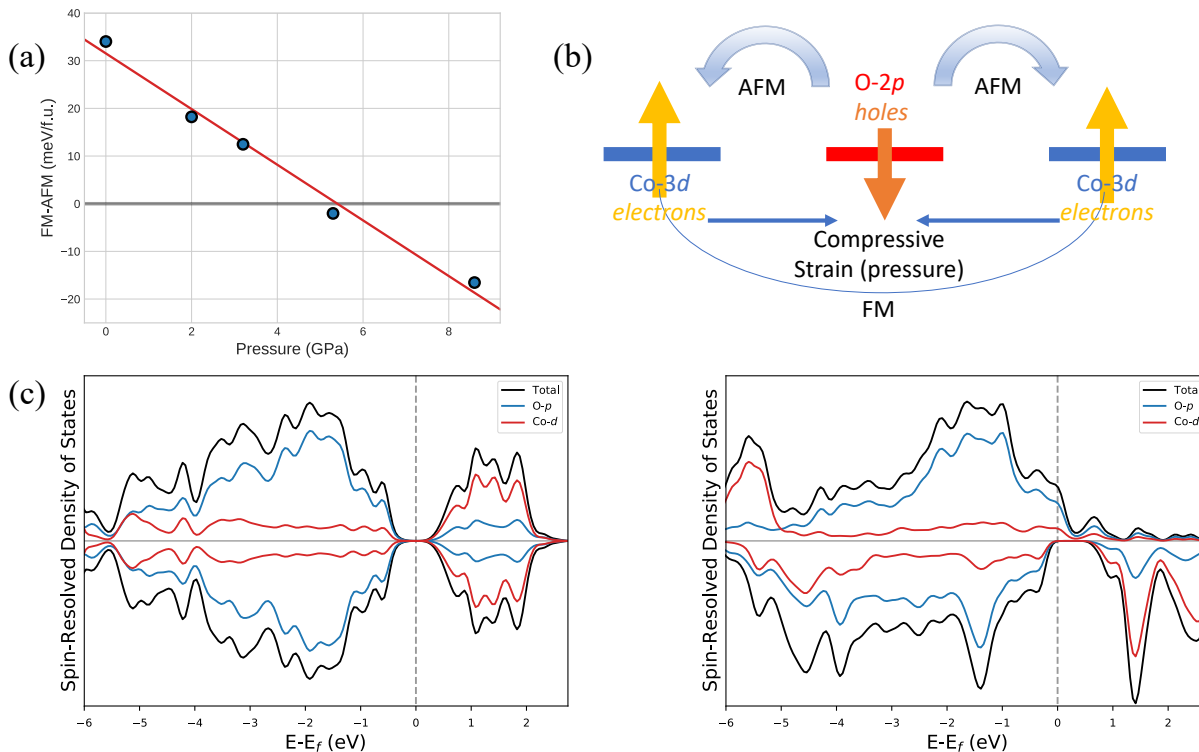


FIG. 3: (a) LDA+ U enthalpy difference in BM-SCO as a function of strain. (b) Scheme of how holes mediate the magnetic transition. (c) LDA+ U DOS plots of AFM insulator and FM metal phases of BM-SCO.

correlated metals, and the band gap is fundamentally controlled by the strength of the charge-transfer energy close to the MIT, and not by the Mott-Hubbard interactions as originally thought for Mottronics applications [52]. While we do not present a rigorously predictive quantitative model that explains all of our observations, we have shown clearly that there exists a linear trend between the calculated band gaps and oxygen occupations across changes in composition, stoichiometry, or pressure. In addition, one could argue that the same trend would be seen for the hybridization between the transition metal and ligand site, which is related to the change in occupation, however hybridization cannot be quantitatively measured in the solid state so we use occupations as a proxy. This knowledge can be used to discover new materials where MIT can be controlled more reliably enabling low-power and efficient neuromorphic devices[4].

ACKNOWLEDGEMENTS

This work was supported by the U.S. Department of Energy, Office of Science, Basic Energy Sciences, Materials Sciences and Engineering Division, as part of the Computational Materials Sciences Program and Center

for Predictive Simulation of Functional Materials. Part of this research was conducted at the Center for Nanophase Materials Sciences (CNMS), which is a DOE Office of Science User Facility. This research used resources of the Oak Ridge Leadership Computing Facility at the Oak Ridge National Laboratory, which is supported by the Office of Science of the U.S. Department of Energy under Contract No. DE-AC05-00OR22725. This research used resources of the National Energy Research Scientific Computing Center, a DOE Office of Science User Facility supported by the Office of Science of the U.S. Department of Energy under Contract No. DE-AC02-05CH11231. This manuscript has been authored by UT-Battelle, LLC under Contract No. DE-AC05-00OR22725 with the U.S. Department of Energy. The United States Government retains and the publisher, by accepting the article for publication, acknowledges that the United States Government retains a nonexclusive, paid-up, irrevocable, worldwide license to publish or reproduce the published form of this manuscript, or allow others to do so, for United States Government purposes. The Department of Energy will provide public access to these results of federally sponsored research in accordance with the DOE Public Access Plan (<http://energy.gov/downloads/oe-public-access-plan>).

C.B. and G.H. contributed equally to this work.

-
- [1] Y. Zhou and S. Ramanathan, *Proceedings of the IEEE* **103**, 1289 (2015).
- [2] J. L. Andrews, D. A. Santos, M. Meyyappan, R. S. Williams, and S. Banerjee, *Trends in Chemistry* **1**, 711 (2019).
- [3] S. Zhang and G. Galli, *npj Computational Materials* **6**, 1 (2020).
- [4] K. Zhang, J. Wang, Y. Huang, L.-Q. Chen, P. Ganesh, and Y. Cao, *npj Computational Materials* **6**, 198 (2020).
- [5] M. Imada, A. Fujimori, and Y. Tokura, *Reviews of modern physics* **70**, 1039 (1998).
- [6] G. Grüner, *Reviews of modern physics* **60**, 1129 (1988).
- [7] U. Staub, G. Meijer, F. Fauth, R. Allenspach, J. Bednorz, J. Karpinski, S. Kazakov, L. Paolasini, and F. d'Acapito, *Physical review letters* **88**, 126402 (2002).
- [8] M. Hepting, M. Minola, A. Frano, G. Cristiani, G. Logvenov, E. Schierle, M. Wu, M. Bluschke, E. Weschke, H.-U. Habermeyer, *et al.*, *Physical Review Letters* **113**, 227206 (2014).
- [9] R. Scherwitzl, S. Gariglio, M. Gabay, P. Zubko, M. Gibert, and J.-M. Triscone, *Physical Review Letters* **106**, 246403 (2011).
- [10] Q. Lu and B. Yildiz, *Nano letters* **16**, 1186 (2016).
- [11] N. Lu, P. Zhang, Q. Zhang, R. Qiao, Q. He, H.-B. Li, Y. Wang, J. Guo, D. Zhang, Z. Duan, *et al.*, *Nature* **546**, 124 (2017).
- [12] H. Jeon, W. S. Choi, M. D. Biegalski, C. M. Folkman, I.-C. Tung, D. D. Fong, J. W. Freeland, D. Shin, H. Ohta, M. F. Chisholm, *et al.*, *Nature materials* **12**, 1057 (2013).
- [13] W. S. Choi, H. Jeon, J. H. Lee, S. A. Seo, V. R. Cooper, K. M. Rabe, and H. N. Lee, *Physical review letters* **111**, 097401 (2013).
- [14] F. Hong, B. Yue, Z. Liu, B. Chen, and H.-K. Mao, *Physical Review B* **95**, 024115 (2017).
- [15] S. Chowdhury, A. Jana, R. Choudhary, and D. Phase, *arXiv preprint arXiv:1905.11645* (2019).
- [16] R. Jaramillo, S. D. Ha, D. Silevitch, and S. Ramanathan, *Nature Physics* **10**, 304 (2014).
- [17] V. Bisogni, S. Catalano, R. J. Green, M. Gibert, R. Scherwitzl, Y. Huang, V. N. Strocov, P. Zubko, S. Balandeh, J.-M. Triscone, *et al.*, *Nature Communications* **7**, 1 (2016).
- [18] J. Shamblin, M. Heres, H. Zhou, J. Sangoro, M. Lang, J. Neuefeind, J. Alonso, and S. Johnston, *Nature communications* **9**, 1 (2018).
- [19] J. Torrance, P. Lacorre, A. Nazzal, E. Ansaldo, and C. Niedermayer, *Physical Review B* **45**, 8209 (1992).
- [20] H. Guo, Z. W. Li, L. Zhao, Z. Hu, C. F. Chang, C.-Y. Kuo, W. Schmidt, A. Piovano, T. W. Pi, O. Sobolev, D. I. Khomskii, L. H. Tjeng, and A. C. Komarek, *Nature Communications* **9**, 43 (2018).
- [21] J. Shi, Y. Zhou, and S. Ramanathan, *Nature Communications* **5**, 4860 (2014).
- [22] H.-T. Zhang, F. Zuo, F. Li, H. Chan, Q. Wu, Z. Zhang, B. Narayanan, K. Ramadoss, I. Chakraborty, G. Saha, G. Kamath, K. Roy, H. Zhou, A. A. Chubykin, S. K. R. S. Sankaranarayanan, J. H. Choi, and S. Ramanathan, *Nature Communications* **10**, 1651 (2019).
- [23] J. Zaanen, G. Sawatzky, and J. Allen, *Physical review letters* **55**, 418 (1985).
- [24] I. Kylänpää, J. Balachandran, P. Ganesh, O. Heinonen, P. R. C. Kent, and J. T. Krogel, *Physical Review Materials* **1** (2017), 10.1103/PhysRevMaterials.1.065408.
- [25] I. Kylänpää, Y. Luo, O. Heinonen, P. R. C. Kent, and J. T. Krogel, *Phys. Rev. B* **99**, 075154 (2019).
- [26] P. Ganesh, F. Lechermann, I. Kylänpää, J. T. Krogel, P. R. C. Kent, and O. Heinonen, *Phys. Rev. B* **101**, 155129 (2020).
- [27] Q. Lu, C. Sohn, G. Hu, X. Gao, M. F. Chisholm, I. Kylänpää, J. T. Krogel, P. R. C. Kent, O. Heinonen, P. Ganesh, and H. N. Lee, *Scientific Reports* **10**, 18554 (2020).
- [28] H. Shin, Y. Luo, P. Ganesh, J. Balachandran, J. T. Krogel, P. R. C. Kent, A. Benali, and O. Heinonen, *Phys. Rev. Materials* **1**, 073603 (2017).
- [29] F. Wrobel, H. Park, C. Sohn, H.-W. Hsiao, J.-M. Zuo, H. Shin, H. N. Lee, P. Ganesh, A. Benali, P. R. C. Kent, O. Heinonen, and A. Bhattacharya, *Phys. Rev. B* **101**, 195128 (2020).
- [30] P. C. Rogge, R. U. Chandrasena, A. Cammarata, R. J. Green, P. Shafer, B. M. Lefler, A. Huon, A. Arab, E. Arenholz, H. N. Lee, *et al.*, *Physical Review Materials* **2**, 015002 (2018).
- [31] J. Kuneš, V. Křápek, N. Parragh, G. Sangiovanni, A. Toschi, and A. Kozhevnikov, *Physical review letters* **109**, 117206 (2012).
- [32] R. Grimm and R. Storer, *Journal of Computational Physics* **7**, 134 (1971).
- [33] W. M. C. Foulkes, L. Mitas, R. J. Needs, and G. Rajagopal, *Rev. Mod. Phys.* **73**, 33 (2001).
- [34] M. Cococcioni and S. De Gironcoli, *Physical Review B* **71**, 035105 (2005).
- [35] P. Giannozzi, S. Baroni, N. Bonini, M. Calandra, R. Car, C. Cavazzoni, D. Ceresoli, G. L. Chiarotti, M. Cococcioni, I. Dabo, A. D. Corso, S. de Gironcoli, S. Fabris, G. Fratesi, R. Gebauer, U. Gerstmann, C. Gougoussis, A. Kokalj, M. Lazzeri, L. Martin-Samos, N. Marzari, F. Mauri, R. Mazzarello, S. Paolini, A. Pasquarello, L. Paulatto, C. Sbraccia, S. Scandolo, G. Sclauzero, A. P. Seitsonen, A. Smogunov, P. Umari, and R. M. Wentzcovitch, *Journal of Physics: Condensed Matter* **21**, 395502 (2009).
- [36] G. Kresse and J. Hafner, *Phys. Rev. B* **47**, 558 (1993).
- [37] G. Kresse and J. Hafner, *Phys. Rev. B* **49**, 14251 (1994).
- [38] G. Kresse and J. Furthmüller, *Computational Materials Science* **6**, 15 (1996).
- [39] G. Kresse and J. Furthmüller, *Phys. Rev. B* **54**, 11169 (1996).
- [40] J. Kim, A. D. Baczewski, T. D. Beaudet, A. Benali, M. C. Bennett, M. A. Berrill, N. S. Blunt, E. J. L. Borda, M. Casula, D. M. Ceperley, S. Chiesa, B. K. Clark, R. C. Clay, K. T. Delaney, M. Dewing, K. P. Esler, H. Hao, O. Heinonen, P. R. C. Kent, J. T. Krogel, I. Kylänpää, Y. W. Li, M. G. Lopez, Y. Luo, F. D. Malone, R. M. Martin, A. Mathuriya, J. McMinis, C. A. Melton, L. Mitas, M. A. Morales, E. Neuscamman, W. D. Parker, S. D. P. Flores, N. A. Romero, B. M. Rubenstein, J. A. R. Shea, H. Shin, L. Shulenburger, A. F. Tillack, J. P. Townsend, N. M. Tubman, B. V. D. Goetz, J. E. Vincent, D. C. Yang, Y. Yang, S. Zhang, and L. Zhao, *Journal of Physics: Condensed Matter* **30**, 195901 (2018).
- [41] P. R. C. Kent, A. Annaberdiyev, A. Benali, M. C.

- Bennett, E. J. Landinez Borda, P. Doak, H. Hao, K. D. Jordan, J. T. Krogel, I. Kylänpää, J. Lee, Y. Luo, F. D. Malone, C. A. Melton, L. Mitas, M. A. Morales, E. Neuscamman, F. A. Reboredo, B. Rubenstein, K. Saritas, S. Upadhyay, G. Wang, S. Zhang, and L. Zhao, *The Journal of Chemical Physics* **152** (2020), 10.1063/5.0004860.
- [42] J. T. Krogel, *Computer Physics Communications* **198**, 154 (2016).
- [43] “Data for this paper, published in the Materials Data Facility ,” <https://doi.org/10.18126/yec3-xn27>.
- [44] A. Jain, G. Hautier, S. P. Ong, C. J. Moore, C. C. Fischer, K. A. Persson, and G. Ceder, *Phys. Rev. B* **84**, 045115 (2011).
- [45] W. Koehler and E. Wollan, *Journal of Physics and Chemistry of Solids* **2**, 100 (1957).
- [46] A. Muñoz, C. de la Calle, J. A. Alonso, P. M. Botta, V. Pardo, D. Baldomir, and J. Rivas, *Phys. Rev. B* **78**, 054404 (2008).
- [47] W. S. Choi, H. Jeon, J. H. Lee, S. S. A. Seo, V. R. Cooper, K. M. Rabe, and H. N. Lee, *Phys. Rev. Lett.* **111**, 097401 (2013).
- [48] M. D. Scafetta, Y. J. Xie, M. Torres, J. E. Spanier, and S. J. May, *Applied Physics Letters* **102**, 081904 (2013), <https://doi.org/10.1063/1.4794145>.
- [49] K. Maiti and D. D. Sarma, *Phys. Rev. B* **54**, 7816 (1996).
- [50] J. L. Cohn, arXiv preprint arXiv:cond-mat/0003047 (Proceedings of the 25th International Thermal Conductivity Conference) (2000).
- [51] A. B. Georgescu, P. Ren, A. R. Toland, E. A. Olivetti, N. Wagner, and J. M. Rondinelli, (2020), arXiv:2010.13306 [cond-mat.mtrl-sci].
- [52] J. Chen, W. Mao, L. Gao, F. Yan, T. Yajima, N. Chen, Z. Chen, H. Dong, B. Ge, P. Zhang, X. Cao, M. Wilde, Y. Jiang, T. Terai, and J. Shi, *Advanced Materials* **32**, 1905060 (2020).

Supplementary Information:

Origin of Metal-Insulator Transitions in Correlated Perovskite Metals

M. Chandler Bennett,^{1,*} Guoxiang Hu,^{2,†} Guangming Wang,³ Olle Heinonen,⁴ Paul R. C. Kent,⁵ Jaron T. Krogel,^{1,‡} and P. Ganesh^{6,§}

¹*Materials Science and Technology Division, Oak Ridge National Laboratory, Oak Ridge, Tennessee 37831, USA*

²*Department of Chemistry and Biochemistry, Queens College, City University of New York, Flushing, NY 11367, USA*

³*Department of Physics, North Carolina State University, Raleigh, North Carolina 27695, USA*

⁴*Materials Science Division, Argonne National Laboratory, Chicago, Illinois USA*

⁵*Computational Sciences and Engineering Division,*

Oak Ridge National Laboratory, Oak Ridge, Tennessee 37831, USA

⁶*Center for Nanophase Materials Sciences, Oak Ridge National Laboratory, Oak Ridge, Tennessee 37831, USA[§]*

(Dated: January 26, 2022)

I. METHODS

A. DFT+U

Density functional theory (DFT) calculations were performed using the Quantum Espresso (QE) software package. The GBRV pseudopotentials and local density approximation (LDA) exchange correlations (XC) were used. The plane wave cutoff was set to 120 Ry for the wave function. Energies were converged with a 1×10^{-7} Ry tolerance. The experimental structures of the perovskites from Inorganic Crystal Structure Database (ICSD) were used for the calculations. The primitive cell of SrCoO₃, LaNiO₃, LaFeO₃, and LaCrO₃ contains 5, 10, 20, and 20 atoms, respectively. An $8 \times 8 \times 8$ k-point grid was used for the 5-atom and 10-atom cells, while an $8 \times 8 \times 5$ k-point grid was used for the 20-atom cell. The primitive cell of the oxygen deficient brownmillerite (BM) SrCoO_{2.5} contains 36 atoms, and a $2 \times 6 \times 6$ k-point grid was used. The magnetic orderings of the experimental ground state were considered, namely ferromagnetic (FM) for SrCoO₃; antiferromagnetic (AFM) for LaFeO₃, LaCrO₃, and BM SrCoO_{2.5}.

The self-consistent Hubbard U (U_{LR}) was calculated from first-principles by using the linear response approach proposed by Cococcioni and Gironcoli, in which U is determined by the difference between the screened and bare second derivative of the energy with respect to localized state occupations. The obtained U_{LR} values are 5.4 eV for Co in SrCoO₃, 4.2 eV for Ni in LaNiO₃, 5.6 eV for Fe in LaFeO₃, and 4.8 eV for Cr in LaCrO₃. For BM SrCoO_{2.5}, there are two types of Co sites, and the U_{LR} was determined to be 6.3 eV for the octahedral Co site and 4.9 eV for the tetrahedral Co site.

B. QMC

For this study, we utilized FN-DMC to obtain ground state properties of the selected family of ABO_x materials. We also calculated excited states for the set of insulating systems. The high-performance QMC code, QMCPACK, was used for all FN-DMC calculations. The QE software package was used throughout to generate the single-body orbitals that define the nodal hypersurface of the FN-DMC wave function.

To reach minimal fixed-node error, we variationally optimized the strength of a metal-site Hubbard interaction within LDA+U for the full set of materials. In the case of BM SrCoO_{2.5}, the U value of the tetrahedral Co site was varied while keeping the difference between its value and the U value at the octahedral site fixed at the difference predicted by linear response ($6.3 - 4.9 \text{ eV} = 1.4 \text{ eV}$). For bulk SrCoO₃, we carefully verified that our LDA+U orbitals were converged to the ground state by uniformly sampling the starting occupation matrix for the Co site within LDA+U. We generated 36 configurations, where all 10 orbital occupations (5 within each spin-channel) were randomly chosen between 0 and 1 over a uniform distribution. Furthermore, for SrCoO₃ we performed a more thorough nodal optimization by including scans over PBE+U and PBE0_w orbital sets, where line searches were performed over U and the exact exchange fraction, w, of PBE0.

For the pseudopotentials, we employed the well-tested high-accuracy correlation-consistent ECPs (ccECPs) [1–5], where available. In cases where ccECPs were not available, namely La and Sr, we generated the pseudopotentials as part of this work. For the La and Sr pseudopotentials, we used a many-body testing protocol consistent with what was defined in the development of ccECPs to verify their accuracy. The ccECPs Fe, Co, and Ni were softened to reach lower kinetic energy cutoff values and consequently lower computational cost. To soften these atoms, their semi-local Gaussian parameter values were tuned to reduce the potential's amplitude at the origin in order to make them less plane-wave hard than were re-

* bennettcc@ornl.gov

† ghu@qc.cuny.edu

‡ krogeljt@ornl.gov

§ ganeshp@ornl.gov

optimized within the full ccECP framework. A cutoff of 730 Ry was used for LaCrO_3 and all other materials used 670 Ry – leading to convergences of 0.05–0.06 mHa/atom for all systems. For self-consistency, an electronic convergence tolerance of 1×10^{-10} Ry was used throughout. For SrCoO_3 , the SCF density was energetically converged to 0.01 mHa/atom using a $12 \times 12 \times 12$ Monkhorst-Pack grid. For all other systems, Monkhorst-Pack grids were used that were commensurate with the $12 \times 12 \times 12$ grid of SrCoO_3 .

Experimental structures were taken from the ICSD database for the full set of materials. The system-specific ICSD collection codes that were used are as follows: SrCoO_3 (77142), LaNiO_3 (173477), $\text{SrCoO}_{2.5}$ (162241), LaFeO_3 (184304), and LaCrO_3 (194033). One-body finite-size effects were minimized by employing twist-averaged boundary conditions. Fine supertwist grids with spacings of less than $0.15/\text{\AA}$ were used for all twist-averaged quantities. Two-body finite size effects were partly reduced through the use of tiled supercells. Supercells containing 8 formula units were used for all the materials – 40 atoms in the case of SrCoO_3 . Cubic supercells were used when possible, namely, for SrCoO_3 , LaFeO_3 , and LaCrO_3 . For LaNiO_3 and BM $\text{SrCoO}_{2.5}$, we performed a brute force search over tiling matrix variations to find near-cubic supercells.

TABLE I. Metal charges from radial density integration from DMC/LDA+ U_{min} . r_{max} is taken to be the outer minima of the spherically averaged total charge density centered at the cation.

system	atom	r_{max} (Å)	Charge (a.u.)	State (a.u.)
SrCoO_3	Co	0.96	14.3513	2.6487
LaNiO_3 (FM)	Ni	1.02	16.2730	1.7270
$\text{SrCoO}_{2.5}$	Co1	1.03	14.6202	2.3798
$\text{SrCoO}_{2.5}$	Co2	1.03	14.7639	2.2361
LaFeO_3	Fe	1.00	13.4973	2.5027
LaCrO_3	Cr	0.99	11.2228	2.7772

TABLE II. Metal charges from radial density integration from LDA+ U_{min} /DMC

system	atom	rcut (Å)	Charge (a.u.)	State (a.u.)
SrCoO_3	Co	1.0	14.5941	2.4059
LaNiO_3	Ni	1.0	16.1558	1.8061
$\text{SrCoO}_{2.5}$	Co1	1.0	14.4792	2.5208
$\text{SrCoO}_{2.5}$	Co2	1.0	14.6142	2.3858
LaFeO_3	Fe	1.0	13.5023	2.4977
LaCrO_3	Cr	1.0	11.2671	2.7329

C. Cohesive Energies

-
- [1] M. C. Bennett, C. A. Melton, A. Annaberdiyev, G. Wang, L. Shulenburg, and L. Mitas, *The Journal of Chemical Physics* **147**, 224106 (2017).
- [2] M. C. Bennett, G. Wang, A. Annaberdiyev, C. A. Melton, L. Shulenburg, and L. Mitas, *The Journal of Chemical Physics* **149**, 104108 (2018).
- [3] A. Annaberdiyev, G. Wang, C. A. Melton, M. Chandler Bennett, L. Shulenburg, and L. Mitas, *The Journal of Chemical Physics* **149**, 134108 (2018).
- [4] G. Wang, A. Annaberdiyev, C. A. Melton, M. C. Bennett, L. Shulenburg, and L. Mitas, *The Journal of Chemical Physics* **151**, 144110 (2019).
- [5] A. Annaberdiyev, C. A. Melton, M. C. Bennett, G. Wang, and L. Mitas, *Journal of Chemical Theory and Computation* **16**, 1482 (2020).
- [6] J. Cheng, A. Navrotsky, X.-D. Zhou, and H. U. Anderson, *Journal of Materials Research* **20**, 191–200 (2005).
- [7] B. J. Boyle, E. G. King, and K. C. Conway, *Journal of the American Chemical Society* **76**, 3835 (1954), <https://doi.org/10.1021/ja01643a072>.
- [8] *Journal of the American Chemical Society* **131**, 12862 (2009), pMID: 19658382, <https://doi.org/10.1021/ja906434c>.

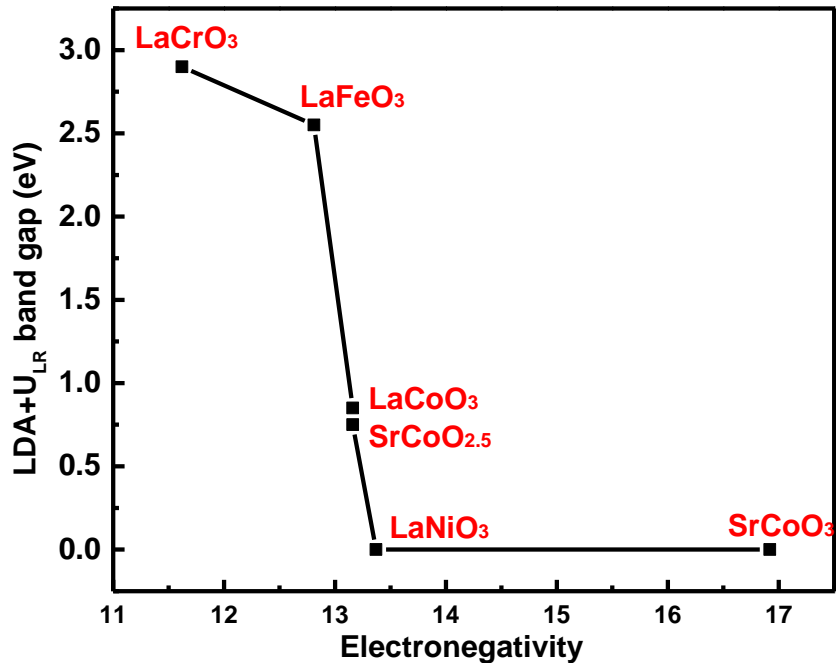


FIG. 1. Band gap of ABO_x as a function of the electronegativity of the B site cation.

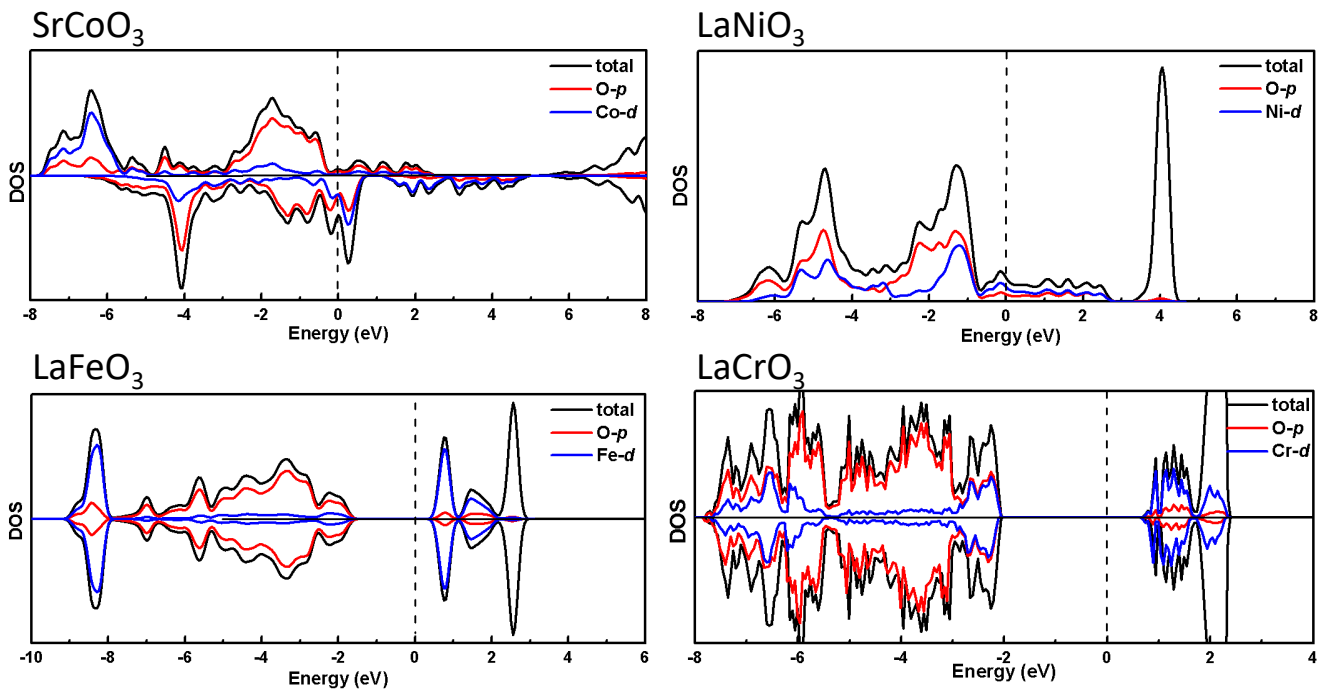


FIG. 2. DOS plots for $SrCoO_3$, $LaNiO_3$, $LaFeO_3$, and $LaCrO_3$. A gap-nature changing from p-p to p-d type can be observed.

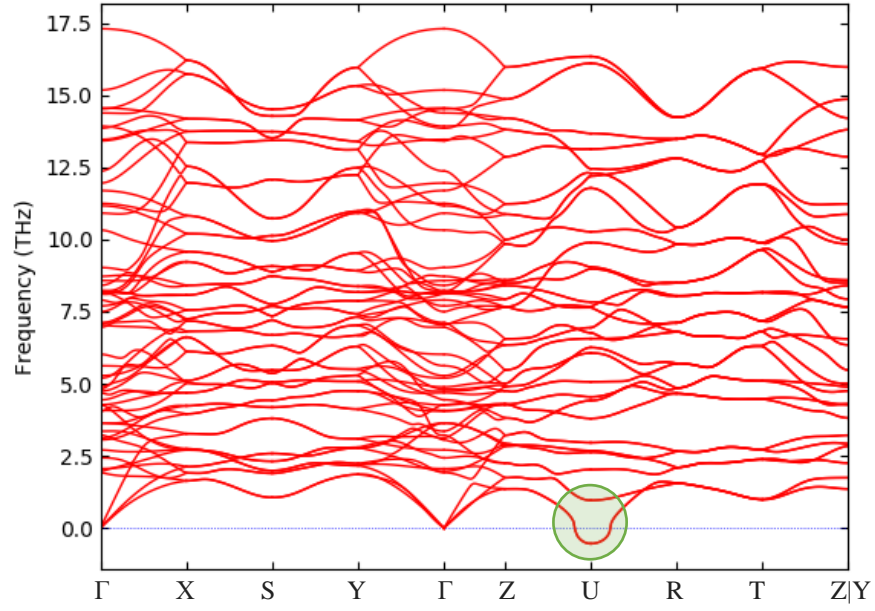


FIG. 3. Phonon dispersions of the hole-doped LaFeO₃.

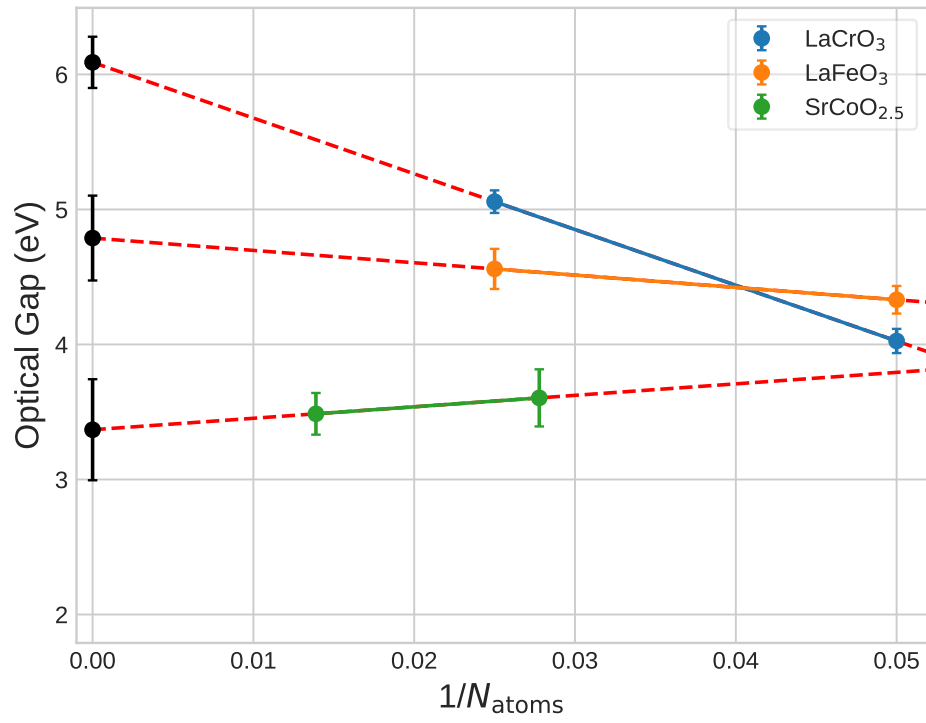


FIG. 4. DMC optical gaps of LaCrO₃, LaFeO₃, and SrCoO_{2.5} extrapolated to thermodynamic limit.

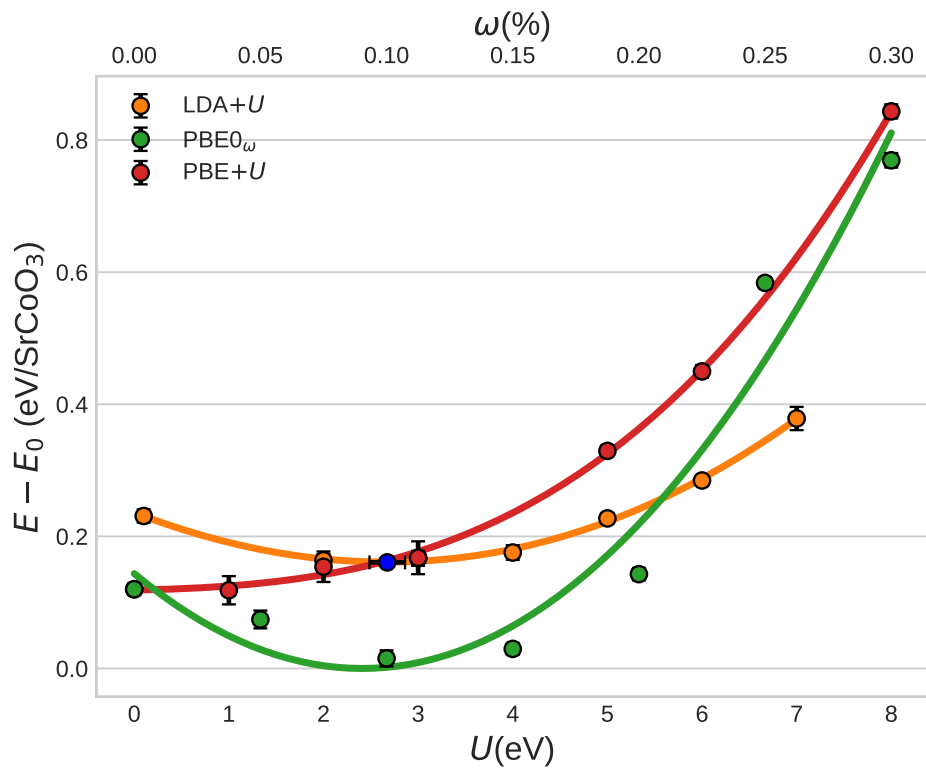


FIG. 5. DMC/LDA+ U nodal optimization of SrCrO_3 using 40 atom simulation cell.

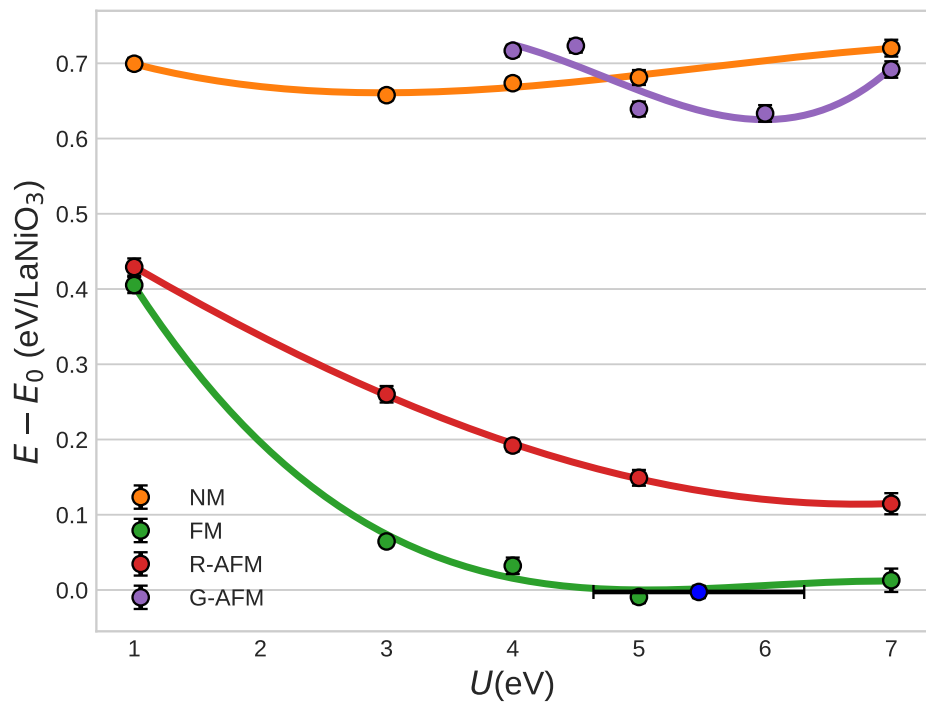


FIG. 6. DMC/LDA+ U nodal optimization of LaNiO_3 using 40 atom simulation cell.

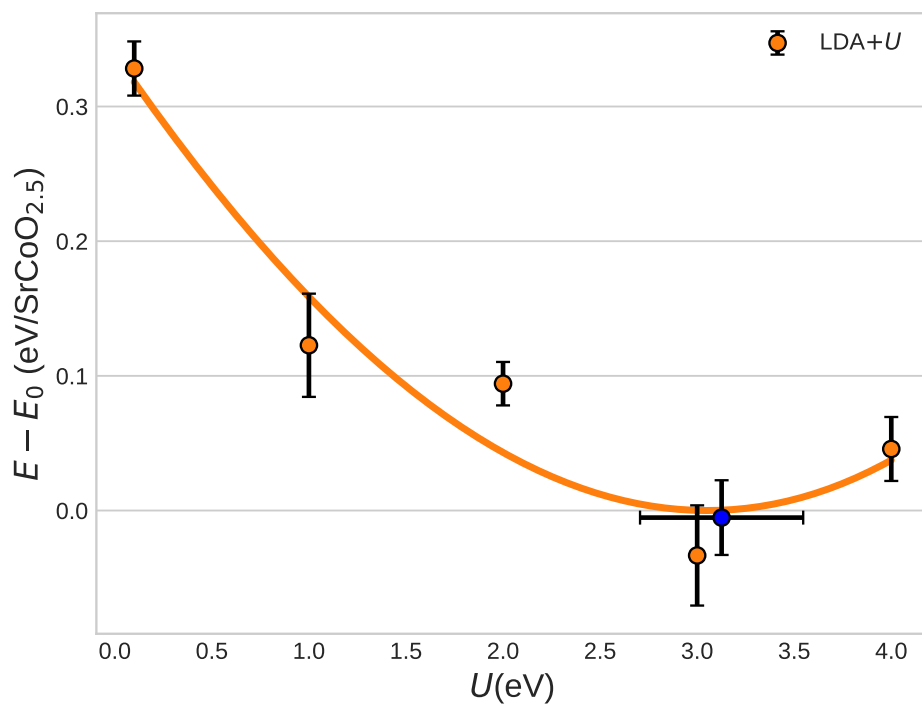


FIG. 7. DMC/LDA+ U nodal optimization of SrCoO_{2.5} using 80 atom simulation cell.

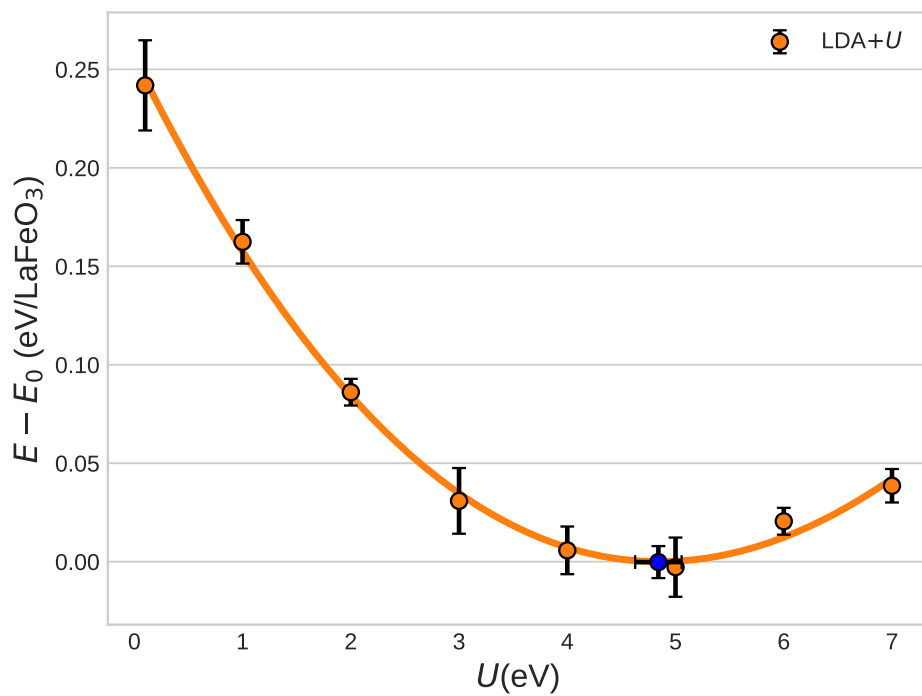


FIG. 8. DMC/LDA+ U nodal optimization of LaCrO₃ using 40 atom simulation cell.

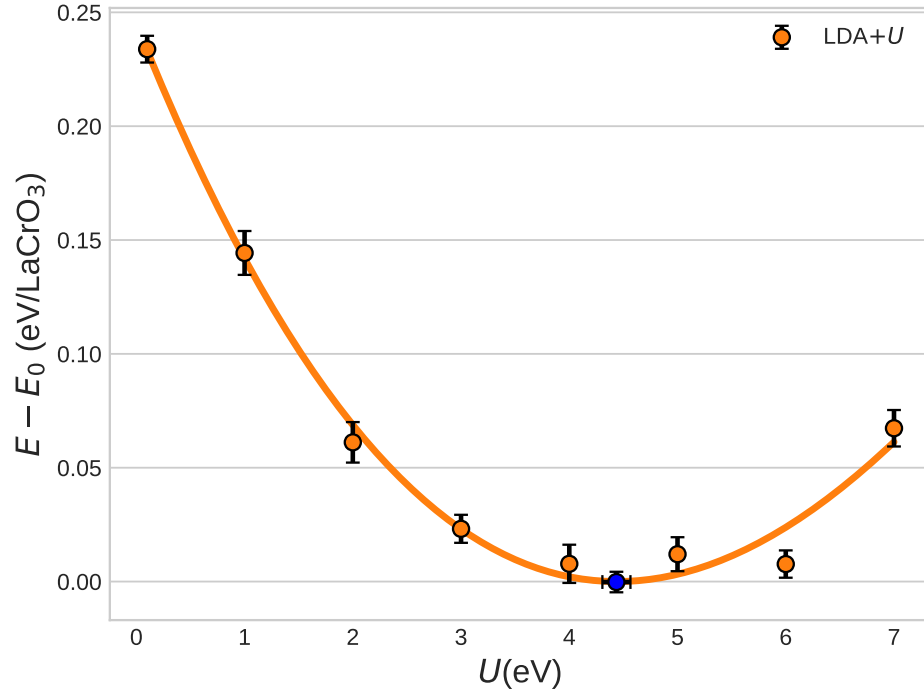


FIG. 9. DMC/LDA+ U nodal optimization of LaFeO₃ using 40 atom simulation cell.

TABLE III. U values predicted from linear response (U_{LR}) and FN-DMC nodal optimizations

system	U_{LR}	U_{min}
SrCoO ₃	5.4.	2.7(2)
LaNiO ₃ (FM)	4.2	5.5(8)
SrCoO _{2.5} (oct/tet)	4.9,6.3	3.1(4),4.5(4)
LaFeO ₃	5.6	4.8(2)
LaCrO ₃	4.8	4.4(1)

TABLE IV. Metal-oxygen bond lengths are listed for each system in Å. The corresponding FN-DMC onsite oxygen charge is also listed in a.u.

system	Bond	Bond Length	Oxygen Charge
SrCoO ₃	O-Co	1.9175	6.4120
LaNiO ₃ (NM)	O1-Ni	1.9378	6.4096
LaNiO ₃ (NM)	O2-Ni	1.9378	6.4021
LaNiO ₃ (FM)	O1-Ni	1.9378	6.4237
LaNiO ₃ (FM)	O2-Ni	1.9378	6.4193
SrCoO _{2.5}	O1-Co1	1.9407	6.4441
SrCoO _{2.5}	O2-Co2	1.7900	6.3741
SrCoO _{2.5}	O3-Co2	1.7947	6.3365
LaFeO ₃	O1-Fe	2.0077	6.5845
LaFeO ₃	O2-Fe	2.0000	6.4333
LaCrO ₃	O1-Cr	1.9687	6.6497
LaCrO ₃	O2-Cr	1.9634	6.4646

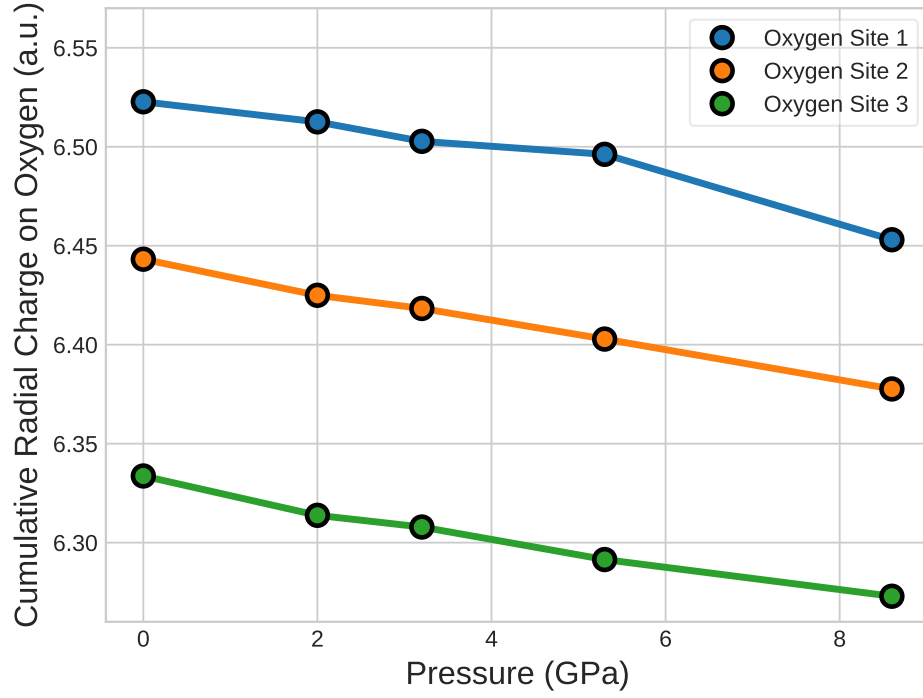


FIG. 10.

TABLE V. Oxygen charges from radial density integration from LDA+ U_{\min} /DMC

system	atom	rcut (\AA)	Charge (a.u.)
SrCoO ₃	O	1.1	6.32684
LaNiO ₃	O	1.1	6.31259
SrCoO _{2.5}	O1	1.1	6.34444
SrCoO _{2.5}	O2	1.1	6.23610
SrCoO _{2.5}	O3	1.1	6.25541
LaFeO ₃	O1	1.1	6.49029
LaFeO ₃	O2	1.1	6.34051
LaCrO ₃	O1	1.1	6.56356
LaCrO ₃	O2	1.1	6.37763

TABLE VI. Oxygen charges from radial density integration from DMC/LDA+ U_{\min}

system	atom	rcut (\AA)	Charge (a.u.)
SrCoO ₃	O	1.1	6.41249
LaNiO ₃	O1	1.1	6.40959
LaNiO ₃	O2	1.1	6.40214
SrCoO _{2.5}	O1	1.1	6.44413
SrCoO _{2.5}	O2	1.1	6.37409
SrCoO _{2.5}	O3	1.1	6.33649
LaFeO ₃	O1	1.1	6.58540
LaFeO ₃	O2	1.1	6.43631
LaCrO ₃	O1	1.1	6.64961
LaCrO ₃	O2	1.1	6.46568

TABLE VII. On-site charges from LDA+U GBRV linear response

system	pressure	Löwdin- U_{LR}				
		TM1	TM2	O1	O2	O3
LaCrO ₃	0	10.7008	12.4225	6.5860	6.5897	
LaFeO ₃	0	10.4151	15.238	6.4192	6.4227	
LaNiO ₃	0	10.4031	17.7272	6.2656		
SrCoO ₃	0	9.6326	16.5942	6.2383		
SrCoO _{2.5}	0	9.6610	16.4557	6.3590	6.3409	6.3353
SrCoO _{2.5}	2	9.6766	16.4644	6.3544	6.3344	6.3271
SrCoO _{2.5}	3.2	9.6874	16.4692	6.3519	6.3306	6.3233
SrCoO _{2.5}	5.2	9.6864	16.4764	6.3481	6.3257	6.3145
SrCoO _{2.5}	8.8	9.6833	16.5029	6.3151	6.2977	6.3038

TABLE VIII. Experimental cohesive energies

LaCrO ₃			
Reaction	T(K)	$\Delta_f H^\circ$ (kJ/mol)	$\Delta_f H^\circ$ (eV)
LaCrO ₃ (s)	298	-73.06	-0.757 ^a
Cr ₂ O ₃ (s)	0	-1128.844	-11.700 ^b
La ₂ O ₃ (s)	0	-1787.36	-18.524 ^c
O(g)	0	246.790	2.558 ^b
Cr(g)	0	395.340	4.097 ^b
La(g)	0	431.29	4.470 ^c

$$E_{\text{coh}} = 0.757 + (11.7 + 18.524)/2 + 3(2.558) + 4.097 + 4.47 \text{ eV} = 32.11 \text{ eV}$$

LaFeO ₃			
Reaction	T(K)	$\Delta_f H^\circ$ (kJ/mol)	$\Delta_f H^\circ$ (eV)
LaFeO ₃ (s)	0	-64.58	-0.669 ^a
Fe ₂ O ₃ (s)	0	-819.025	-8.489 ^b
La ₂ O ₃ (s)	0	-1787.36	-18.524 ^c
O(g)	0	246.790	2.558 ^b
Fe(g)	0	413.127	4.282 ^b
La(g)	0	431.29	4.470 ^c

$$E_{\text{coh}} = 0.669 + (8.489 + 18.524)/2 + 3(2.558) + 4.282 + 4.47 \text{ eV} = 30.6 \text{ eV}$$

LaNiO ₃			
Reaction	T(K)	$\Delta_f H^\circ$ (kJ/mol)	$\Delta_f H^\circ$ (eV)
LaNiO ₃ (s)	1000	-46.07	-0.477 ^a
Ni ₂ O ₃ (s)	298	-489.5	-5.073 ^e
La ₂ O ₃ (s)	0	-1787.36	-18.524 ^c
O(g)	0	246.790	2.558 ^b
Ni(g)	0	428.076	4.437 ^b
La(g)	0	431.29	4.470 ^c

$$E_{\text{coh}} = 0.477 + 5.073/2 + 18.524/2 + 3(2.558) + 4.437 + 4.47 \text{ eV} = 28.86 \text{ eV}$$

^a Reference [6]^b JANAF Tables^c <https://data.nist.gov/od/id/mds2-2124>^d Reference [7]^e Reference [8]